BIOCHEMISTRY
including biophysical chemistry & molecular biology

Article

pubs.acs.org/biochemistry

Conformational Flexibility in the Allosteric Regulation of Human UDP-α-D-Glucose 6-Dehydrogenase

Nicholas C. Sennett, Renuka Kadirvelraj, and Zachary A. Wood*

Department of Biochemistry and Molecular Biology, University of Georgia, Athens, Georgia 30602, United States

Supporting Information

ABSTRACT: UDP-α-D-xylose (UDX) acts as a feedback inhibitor of human UDP-α-D-glucose 6-dehydrogenase (hUGDH) by activating an unusual allosteric switch, the Thr131 loop. UDX binding induces the Thr131 loop to translate ~5 Å through the protein core, changing packing interactions and rotating a helix ($\alpha6_{136-144}$) to favor the formation of an inactive hexameric complex. But how does to conformational change occur given the steric packing constraints of the protein core? To answer this question, we deleted Val132 from the Thr131 loop to approximate an intermediate state in the allosteric transition. The 2.3 Å resolution crystal structure of the deletion construct (Δ132) reveals an open conformation that relaxes steric constraints and facilitates repacking of the protein core. Sedimentation velocity studies show that the open conformation stabilizes the Δ132 construct as a hexamer with point group symmetry 32, similar to that of the active complex. In contrast, the UDX-inhibited enzyme forms a lower-symmetry, horseshoe-shaped hexameric complex. We show that the Δ132 and UDX-inhibited structures have similar hexamer-building interfaces, suggesting that the hinge-bending motion represents a path for the allosteric transition between the different hexameric states. On the basis of (i) main chain flexibility and (ii) a model of the conformational change, we propose that hinge bending can occur as a concerted motion between adjacent subunits in the high-symmetry hexamer. We combine these results in a structurally detailed model for allosteric feedback inhibition and substrate−product exchange during the catalytic cycle.

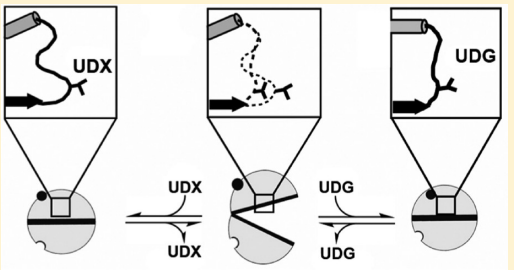

Human UDP-α-D-glucose 6-dehydrogenase (hUGDH) catalyzes the NAD^+-dependent oxidation of UDP-α-D-glucose (UDG) to UDP-α-D-glucuronic acid (UGA).[1] UGA is an essential substrate in the biosynthesis of glycosylaminoglycans (GAGs), which provide tensile strength to the extracellular matrix and serve as contacts for cell adhesion.[2] In addition to their structural roles, GAGs are involved in cell signaling pathways that control replication and differentiation.[3,4] Thus, GAGs are often implicated in metastasis.[4−6] Increased levels of the GAG hyaluronan are strongly correlated with tumor growth and metastasis in breast, colorectal, and prostate cancers.[7−11] In fact, downregulation of hUGDH has been shown to reduce the motility of colorectal cancer cells.[12] Understanding how hUGDH activity is regulated is an important goal in designing new therapies for cancer.

hUGDH is composed of an NAD^+ binding (NB) domain, a dimerization domain and a nucleotide sugar binding (SB) domain (Figure 1A). Three dimers of hUGDH associate to form a hexamer with point group symmetry 32 (Figure 1B).[13,14] The hexamer-building interfaces are formed by packing interactions between adjacent NB and SB domains.[13,14] These interfaces are key to the unusual allosteric inhibition mechanism that regulates hUGDH activity.[13] Unlike typical allosteric enzymes, the active and allosteric sites in hUGDH are combined in a single, bifunctional site.[13] The feedback inhibitor, UDP-α-D-xylose (UDX), competes with the substrate for binding to the active site. UDX lacks the C5′ hydroxymethyl present in UDG, and this single structural difference elicits a distinct induced-fit response that converts hUGDH into an inactive, low-symmetry hexamer (Figure 1B).[13,15] The molecular switch that disrupts the hexamer is a buried loop (the Thr131 loop) that connects the active site to an α-helix ($\alpha6_{136-144}$) in the hexamer-building interface. UDX binding alters the structure of the Thr131 loop, which rotates the $\alpha6_{136-144}$ helix and disrupts the symmetry of the hexamer (Figure 1C,D). Because the active site can bind either substrate or effector with distinct induced-fit conformations, the allosteric mechanism is called allokleidic (allos, "other", and kleidi, "key").[13]

The conformational change of the Thr131 loop can be described as an ~5 Å screwlike translation along an axis represented by the extended main chain (Figure 1C,D). As a result of this translation, the side chains of V132 and P133 rotate ~180° about the main chain and eight buried residues undergo a change in rotameric state.[13] Our previous work has shown that packing defects (cavities and voids) provide conformational freedom to accommodate the alternate packing arrangements of the core,[13] but it was not known how this repacking could occur given the steric constraints of the protein core. To study this transition, we deleted V132 from the Thr131 loop to mimic an intermediate conformational state. Our rationale in the design of the Δ132 construct was as follows. (i) The screwlike translation of the Thr131 loop shifts

Received: September 1, 2011
Revised: September 29, 2011
Published: September 30, 2011

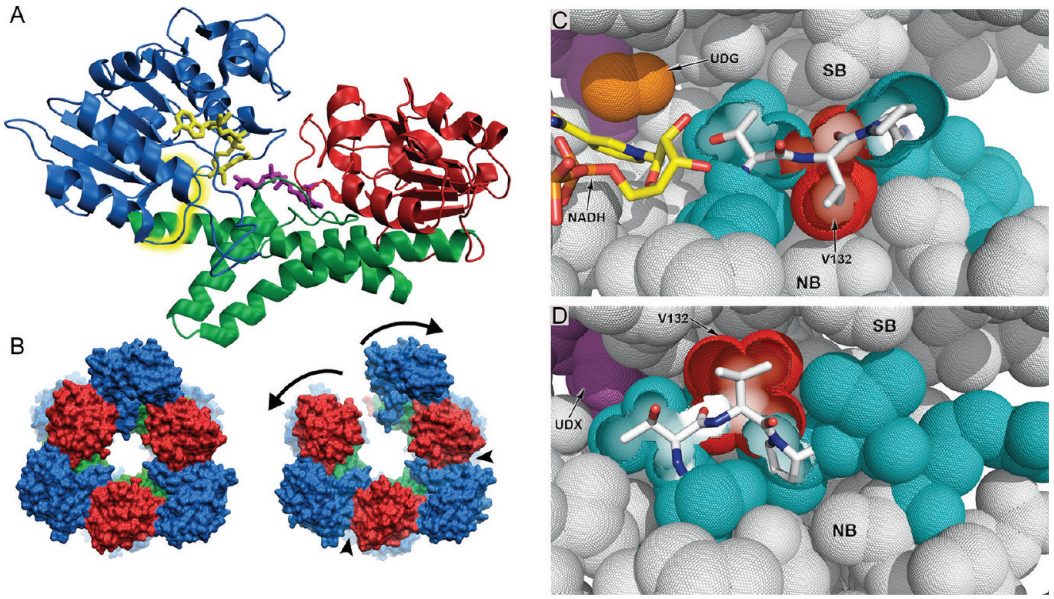

Figure 1. Conformational changes in the regulation of hUGDH activity. The NB (residues 1−212), dimerization (residues 213−322), and SB (residues 323−466) domains are colored blue, green, and red, respectively. (A) Monomer of hUGDH (PDB entry 2Q3E) in complex with UDG (purple) and NADH (yellow). The Thr131 loop is highlighted in yellow. (B) Surface representation of the active, high-symmetry (left) and inhibited, low-symmetry (right) hexameric forms of hUGDH (PDB entries 2Q3E and 3PTZ, respectively). The binding of UDX causes adjacent dimers to rotate ∼10° (curved arrows) about an axis located in the hexamer-building interface (►). (C) Cut-away of the protein core depicting the packing environment (gray spheres) of the Thr131 loop (teal spheres and white sticks) and V132 (red spheres) in the active conformation (PDB entry 2Q3E). The bound NADH (yellow sticks) and UDG (purple spheres with the C5′ hydroxymethyl colored orange) are shown. (D) Packing environment of the inhibited conformation of the Thr131 loop (PDB entry 3PTZ) shown from the same perspective as panel C with UDX (purple spheres). The NAD binding site is occluded by the loop, inactivating the enzyme.

the C_α atom of V132 by ∼5 Å, greater than the C_α−C_α distance in a peptide chain, and (ii) the removal of a residue will flip P133 about the main chain to approximate the screwlike rotation. Because the hUGDH core already facilitates the Thr131 loop translation, we predicted that the deletion would be accommodated. The crystal structure of the Δ132 construct shows that the deletion of V132 has indeed trapped the enzyme in an intermediate conformation in the allokleidic response. On the basis of our results, we propose a structurally detailed model for the transition of the hexamer between the active and inhibited conformations.

MATERIALS AND METHODS

Crystallization and Data Collection. The Δ132 construct and wild-type hUGDH were recombinantly expressed and purified as previously described.[13] Δ132 hUGDH at a concentration of 10 mg/mL was used for hanging drop vapor diffusion crystallization screens. All screens contained 2 μL drops mixed in a 1:1 protein:reservoir ratio. Incubation of hUGDH in 0.1 mM piperine (Sigma), 12% PEG 3350, 2% DMSO, 125 mM magnesium acetate, and 0.1 M sodium glycine (pH 9.4) yielded triangular plates within a week. Crystals were cryoprotected with 20% glycerol, 12% PEG 3350, 2% DMSO, 125 mM magnesium acetate, and 0.1 M sodium glycine (pH 9.4) and flash-cooled in liquid nitrogen. A 2.3 Å resolution data set was collected at beamline 22-ID (SER-CAT) at the Argonne National Laboratory (Argonne, IL) using a MAR 300 mm CCD detector, a wavelength of 1 Å, and an oscillation step of 1.0°. The data were processed in space group C2 using XDS,[16] and 5% of the data was set aside for cross validation. The crystal parameters and data collection statistics are summarized in Table 1.

Structure Solution and Refinement. The Δ132 structure was determined by molecular replacement using AutoMR.[17] The self-rotation function was consistent with 32 symmetry, but initial molecular replacement attempts using the hUGDH:UDG:NADH hexamer (PDB entry 2Q3E) as a search model failed. Suspecting a conformational change because of the deletion, we removed the NB domains (residues 1−212) from the search model and successfully placed the structure using AutoMR. The NB domains were manually docked in density and subjected to rigid body and positional refinement in REFMAC.[18] Refinement consisted of iterative cycles of manual rebuilding using COOT,[19] followed by positional refinement with PHENIX.[20] During refinement in PHENIX, the initial R_{free} test set from REFMAC was corrupted. To decouple the test set and calculate a posteriori R_{free}, we subjected the model to simulated annealing using Cartesian molecular dynamics at 5000 K as described by Brunger et al.[21] The *B* factors were refined using TLS with each domain as a separate group. For domain flexibility analysis, the final structure was re-refined without TLS parameters. All residues of the Δ132 crystal structure were modeled with the exception of the C-terminal tail (residues 466−494), which is disordered in all chains. Refinement statistics are summarized in Table 1.

Sedimentation Velocity. hUGDH (45 μM) was dialyzed for 2 h against 25 mM Tris (pH 8.8), 300 mM KCl, and 1 mM TCEP and then equilibrated to final concentrations of 150 mM KCl and 25 mM Tris (pH 8.5) at 23 °C. After dialysis, hUGDH was diluted to the appropriate concentration, loaded into 12 mm sedimentation velocity cells, and equilibrated for 4 h at 20 °C. Cells were then placed in an An60 Ti rotor and spun in an Optima XLA analytical ultracentrifuge (Beckman Coulter) at 50000 rpm for 8 h. Sedimentation was followed in 0.003 cm step sizes at 230 nm. The density, viscosity, and partial specific volume

Table 1. Data Collection and Refinement Statistics

Data Collection	
space group	*C*2
unit cell dimensions	
a, *b*, *c* (Å)	180.0, 116.9, 96.3
α, *β*, *γ* (deg)	90.0, 115.9, 90.0
completeness (%)	96.4 (91.2)[a]
redundancy	3.6 (3.7)[a]
$I/\sigma I$	18.1 (2.5)[a]
R_{meas}[b] (%)	5.2 (79.0)[a]
R_{pim}[c] (%)	3.4 (43.3)[a]
Refinement	
resolution (Å)	2.3
no. of reflections	280273
R_{work}/R_{free}	0.20/0.23[d]
no. of atoms	10831
protein	10747
water	84
B factor (Å^2)	
protein	68.3
water	57.6
stereochemical ideality	
bond lengths (Å)	0.009
bond angles (deg)	1.05
ϕ and ψ most favored (%)	91.1
ϕ and ψ allowed (%)	8.9
ϕ and ψ generously allowed (%)	0

[a]Values in parentheses are for the highest-resolution shell. [b]R_{meas} is the redundancy-independent merging *R* factor of Diederichs and Karplus.[41] [c]R_{pim} is the precision-indicating merging *R* factor of Weiss and Hilgenfeld.[42] [d]Posteriori calculated R_{free}[21](see Materials and Methods).

were estimated to be 1.00603 g/mL, 0.010068 P, and 0.7384 mL/g, respectively, using SEDNTERP.[22] A best-fit $c(s)$ distribution was modeled using SEDFIT.[23] Systematic and time-invariant noise, baseline, and meniscus were fit.

Kinetics. Enzyme activity was assayed by mixing equal volumes of an enzyme solution [3.6 μM wild-type hUGDH or 18.2 μM Δ132 construct, 5 mM EDTA, 25 mM Tris (pH 8.0), and 150 mM NaCl] with a substrate mix [4 mM NAD^+, 4 mM UDG, 5 mM EDTA, 25 mM Tris (pH 8.0), and 150 mM NaCl]. The enzyme and substrate mixes were preincubated at 25 °C for 10 min and then mixed in a 2 mm quartz cuvette. The final reaction mixture contained 1.8 μM wild-type hUGDH or 9.1 μM Δ132 construct and 2 mM NAD^+, 2 mM UDG, 5 mM EDTA, 25 mM Tris (pH 8.0), and 150 mM NaCl. Enzyme activity was recorded as an increase in absorbance at 340 nm using an Agilent 8453 UV−vis spectrophotometer equipped with a Peltier temperature control set to 25 °C. Time points were measured in 1 s intervals for 10 min. The specific activity was calculated using initial velocities averaged from four replicate reactions. All initial velocity fit lines had R^2 values of 0.99.

RESULTS

Truncation of the Thr131 Loop Stabilizes the Hexameric State of hUGDH. The Δ132 construct was expressed at levels comparable to that of wild-type hUGDH (~25 mg/L) and purified as a soluble protein using our standard conditions. Enzyme assays show that the Δ132 construct is relatively inactive, displaying only 0.07% of the wild-type specific activity (Figure 2A). Using sedimentation velocity, we compared wild-type hUGDH to the Δ132 construct to determine the effects of the V132 deletion on the oligomeric state of the enzyme. At the lowest protein concentration studied (0.4 μM), the sedimentation of wild-type hUGDH is modeled as a single dimeric species (5.7S), although the width and tailing of the distribution indicate a small degree of aggregation (Figure 2B). At 0.9 μM hUGDH, a complex distribution of at least three sedimenting species (5.7S, 8.5S, and 11.0S) is observed. The absence of discrete species suggests an equilibrium among dimeric, tetrameric, and hexameric states. At the highest protein concentration studied (1.5 μM), the distribution shifts toward the hexameric species that has been described previously.[13,24] These data show that wild-type hUGDH undergoes a concentration-dependent association to form the hexamer. In contrast, the Δ132 construct sediments as a single hexameric species (11.8S) at all concentrations studied (Figure 2C).

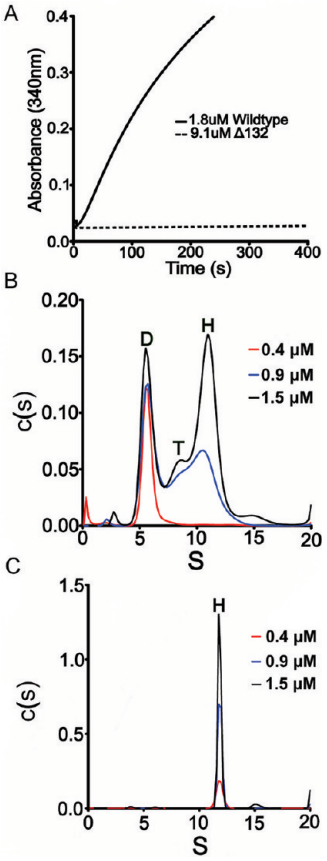

Figure 2. Deletion of V132 stabilizes a low-activity hexamer. (A) Specific activities of the wild type (—) and the Δ132 construct (---) are 1.16 ± 0.03 μmol mg^{-1} min^{-1} and 0.8 ± 0.1 nmol mg^{-1} min^{-1}, respectively. (B) Sedimentation velocity $c(s)$ distributions[23] of wild-type hUGDH at 0.4 (red), 0.9 (blue), and 1.5 μM (black). Peaks corresponding to the dimer (D), tetramer (T), and hexamer (H) are identified. (C) Sedimentation velocity studies of the Δ132 construct analyzed using the same conditions used for wild-type hUGDH in panel B.

The Δ132 hUGDH Crystal Structure Reveals a Hinge-Bending Motion. The crystal structure of the Δ132 construct at 2.3 Å resolution reveals three molecules in the asymmetric unit that are related to each other by a noncrystallographic 3-fold axis of symmetry. The application of a 2-fold crystallographic axis produces a hexamer displaying point

dx.doi.org/10.1021/bi201381e | *Biochemistry* 2011, 50, 9651−9663

group symmetry 32, similar to the previously described hUGDH structures[13,14] (Figure 3A). Despite the deletion of

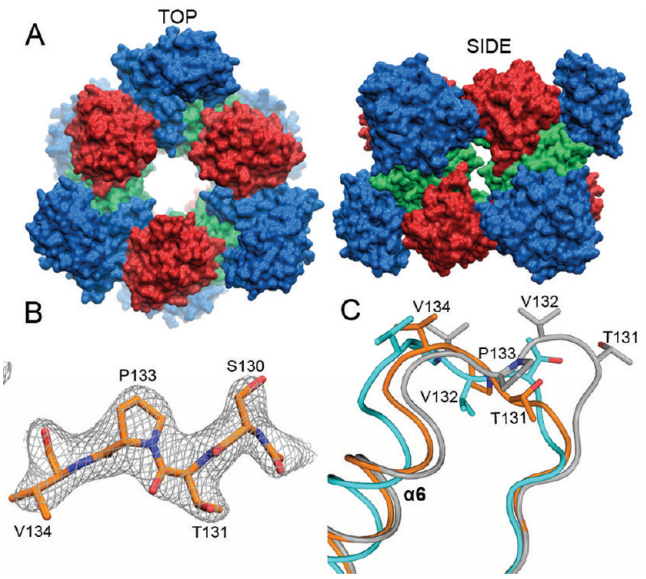

Figure 3. Structure of the Δ132 construct. (A) Solvent accessible surface showing "top" (left) and "side" (right) views of Δ132. The NB (blue), dimerization (green), and SB (red) domains are identified. (B) Difference ($F_o - F_c$) electron density map at 3σ calculated after residues 127−135 had been omitted and the resulting model subjected to simulated annealing. (C) Thr131 loop of the Δ132 construct (orange) compared to the active, high-symmetry (cyan) and UDX-inhibited, low-symmetry (gray) hexameric forms of hUGDH. The α6 switch helix is identified.

V132, the Thr131 loop is well-ordered in the NB domain (Figure 3B). As expected, the Thr131 loop in the Δ132 construct is in a distinct conformation relative to the active and inhibited structures (Figure 3C). In this conformation, the side chain of T131 is rotated away from the active site. Because T131 is a conserved catalytic residue,[14,25] the altered conformation may explain the lower activity of the Δ132 construct (Figure 2A).

A monomer of the Δ132 construct superimposes onto the active complex (hUGDH:UDG:NADH) with a root-mean-square deviation (rmsd) of 2.4 Å for 464 corresponding C_α atoms showing that the NB and SB domains have undergone a significant conformational change (Figure 4A). An analysis of the conformational change using a difference distance matrix[26,27] is consistent with a hinge-bending motion about an axis located between residues 218 and 224 in helix α9 of the dimerization domain (Figure 4B, region III). The difference matrix identifies five regions that share a similar spatial relationship with both terminal domains despite the conformational change (Figure 4B, regions I−V). Using DynDom,[28] we show that the NB domain has rotated 12.3° about a hinge axis located between residues 219 and 220 in helix α9 of the dimerization domain (Figure 4C). We will refer to the Δ132 and hUGDH:UDG:NADH conformations as the "open" and "closed" forms, respectively. All five regions identified in the difference distance matrix are clustered around the rotation axes predicted by DynDom (Figure 4B,C). Recent work by Egger et al. identified a similar hinge-bending motion in the active site mutant, $hUGDH_{T131A}$.[14] Using DynDom, we have identified similar hinge-bending axes in hUGDH:UGA:NAD^+ and the mutant $hUGDH_{E161Q}$ (Table 2 and Figure 4C). We have also examined domain flexibility in distantly related members of the UGDH family. A Dali search[29] identified UDP-*N*-acetylmannosamine dehydrogenase (24% identity, rmsd of 3.4 Å for 405 corresponding C_α atoms) and NDP-*N*-acetyl-D-galactosamine dehydrogenase (24% identity, rmsd of 4.1 Å for 427 corresponding C_α atoms) as homologues. The relatively large structural deviations are the result of a hinge-bending conformational change. A superposition of the corresponding domains in the homologues with hUGDH:UDG:NADH results in rmsds of ≤1.9 Å (Table S1 of the Supporting Information). Using DynDom, we show that the position of the hinge axis in hUGDH is conserved in each of the homologues but the direction of rotation is variable (Figure S1 of the Supporting Information).

Because the Thr131 loop is near the hinge-bending axis, we examined the contribution of the V132 deletion to the open conformation of hUGDH (Figure 4C, region II). We modeled the NB domains of the Δ132 construct in the closed conformation using the hUGDH:UDG:NADH structure (PDB entry 2Q3E) as a template. To do this, we divided the Δ132 structure into an N-terminal fragment (residues 1−212) and a C-terminal fragment (residues 213−466). We superimposed the N- and C-terminal fragments of Δ132 onto the corresponding domains from the hUGDH:UDG:NADH structure (rmsds of 0.50 Å for 211 C_α atoms and 0.56 Å for 253 C_α atoms, respectively). This modeling experiment shows that closing the NB domain of the Δ132 construct would introduce a steric clash between the side chain of K220 and residues T131, P160, and E161 (Figure 5A). In the open conformation, K220 is exposed to solvent and has adopted a rotameric state incompatible with the closed conformation. Assuming K220 adopts the conformation seen in hUGDH:UDG:NADH, the closed domain structure of Δ132 would still be unfavorable because of the burial of the Thr131 O_γ hydroxyl group in a hydrophobic cavity (Figure 5B). This cavity is inaccessible to water in most chains of the hUGDH:UDG:NADH structure. Chain L is an exception; it contains a small channel that may allow a water to be buried with Thr131 (Figure 5B). The burial of a polar residue in a hydrophobic cavity has been estimated to destabilize proteins by ∼1−3 kcal/mol.[30] Because the folded state of a globular protein is typically only 4−15 kcal/mol more stable than the unfolded state,[31] burying the Thr131 O_γ hydroxyl and closure of the NB and SB domains will be unfavorable in the absence of a compensatory, stabilizing interaction.

The NB and SB Domains Display Flexibility While Packed in the Hexameric Complex. The hexamer-building interface in hUGDH is formed by the packing of the NB domain of one monomer against the SB domain of an adjacent subunit (Figure 3A). Because both the open and closed conformations used in the hinge-bending analysis were crystallized as hexamers, we asked if both the NB and SB domains could move in a concerted motion without disrupting the hexameric complex. Superimposing the hexamer-building interfaces of the open and closed conformations shows that both domains have moved to maintain the packing interface (Figure 6A). We used Morphserver[32] to model the hinge-bending motion in the context of the hexamer (Movies S1 and S2 of the Supporting Information). This analysis shows that the SB domain can undergo a small rigid-body rotation in response to the larger motion of the NB domain without disrupting the complex. Importantly, there are no main chain clashes preventing this

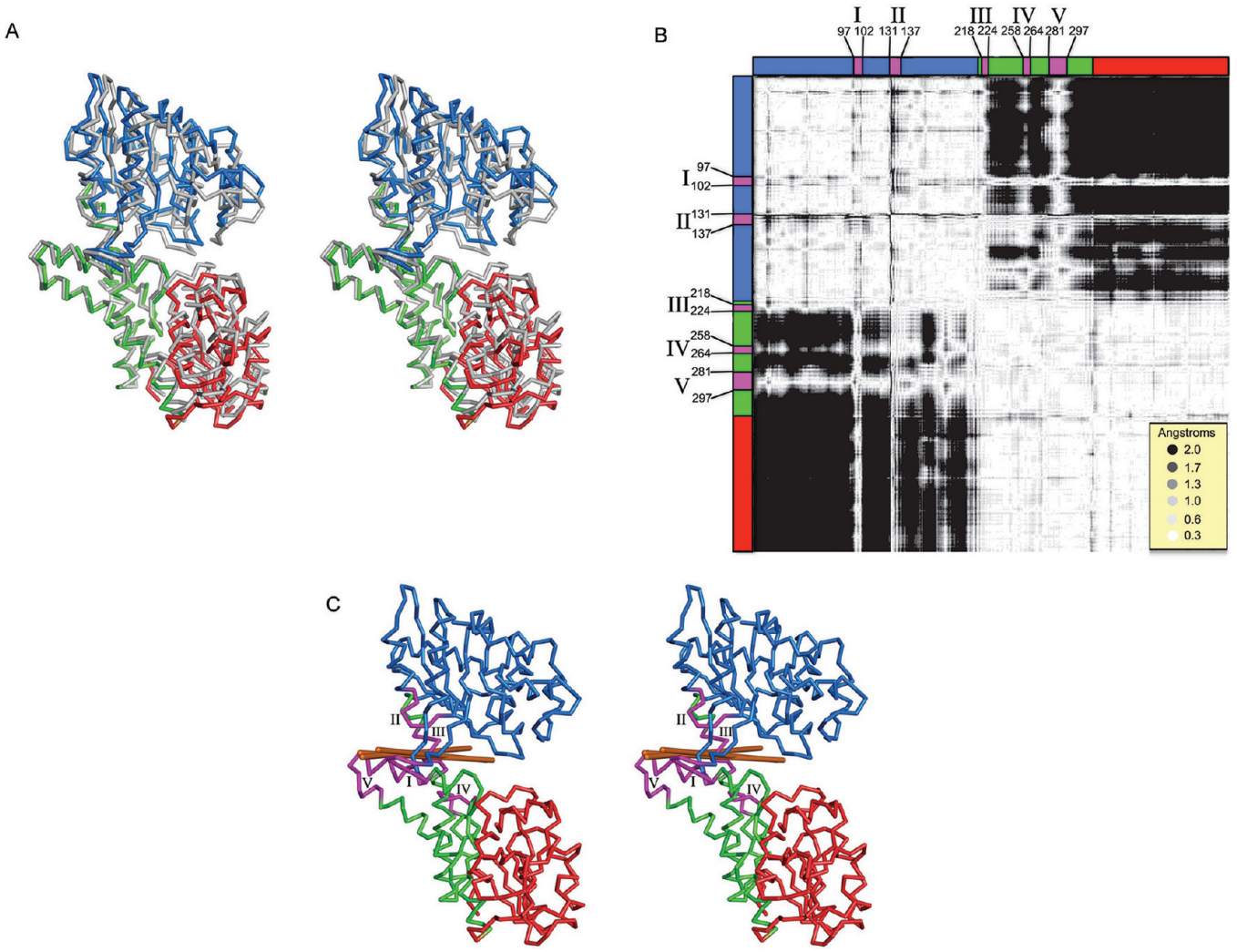

Figure 4. Δ132 structure revealing a hinge-bending conformational change. (A) Superposition of hUGDH:UDG:NADH (gray, PDB entry 2Q3E) with Δ132, revealing a rotation of the NB (blue) and SB (red) domains relative to the dimerization domain (green). (B) Difference distance matrix comparing hUGDH:UDG:NADH with Δ132. Colored bars indicate the domain structure (colored as described above), with potential hinge-bending regions I–V colored purple. The plot was generated using a program kindly provided by P. Fleming.[27] (C) Stereoview of Δ132 with domains colored as described above. The hinge-bending regions (purple) identified in the difference distance plot (panel B) are mapped onto the structure. DynDom identified three similar hinge-bending axes (orange rods) in pairwise comparisons of hUGDH:UDG:NADH (chain A, PDB entry 2Q3E) with (i) Δ132 (chain A), (ii) hUGDH:UGA:NAD^+ (chain B, PDB entry 2QG4), and (iii) $hUGDH_{E161Q}$ (chain A, PDB entry 3KHU). Chain B of 2QG4 was chosen for analysis because chain A is in the closed conformation (details in the text and Table 2).

motion. Still, these conformational changes would require a significant degree of flexibility between the NB and SB domains to prevent disruption of the complex.

We analyzed the *B* factors of hUGDH for evidence of the conformational flexibility required for the concerted motion of both domains. *B* factors are related to the mean-squared amplitude of atomic displacement ($\langle u^2 \rangle$) by the equation $B = 8\pi^2\langle u^2 \rangle$. Because *B* factors reflect the vibrational or static disorder of an atom in a crystalline environment,[33] they are useful indicators of flexibility in a folded protein.[34,35] In a protein that undergoes a hinge-bending motion, the mobile domains will behave as rigid bodies in the crystal lattice and thus will appear as distinct regions of flexibility. Such behavior is observed in the Δ132 crystal structure; the pattern of main chain flexibility indicated by the *B* factors is mirrored in the domain structure of the protein (Figure 7A). We observed the same pattern of flexibility in all 12 chains in the hUGDH:UDG:NADH crystal structure (PDB entry 2Q3E), ruling out any contributions due to the deletion of V132 or crystal packing (data not shown).

In proteins that undergo a hinge-bending conformational change, the main chain *B* factors will display a linear increase with distance from the center of motion[34,35] (Figure 7B, inset).

Table 2. Hinge-Bending Motion in hUGDH

crystal structure[a]	PDB entry	chain	hinge axis	hinge bending (deg)
Δ132	3TF5	A	219–220	12.3
$hUGDH_{E161Q}$	3KHU	A	219–222	9.0
hUGDH:UGA:NAD^+	2QG4	A	219–220	11.4
hUGDH:UGA:NAD^+	2QG4	B	–	0
$hUGDH_{T131A}$	3ITK	A	219–225	13.3

[a]All hinge-bending axes were calculated relative to chain A of PDB entry 2Q3E using DynDom.[28]

dx.doi.org/10.1021/bi201381e | *Biochemistry* 2011, 50, 9651–9663

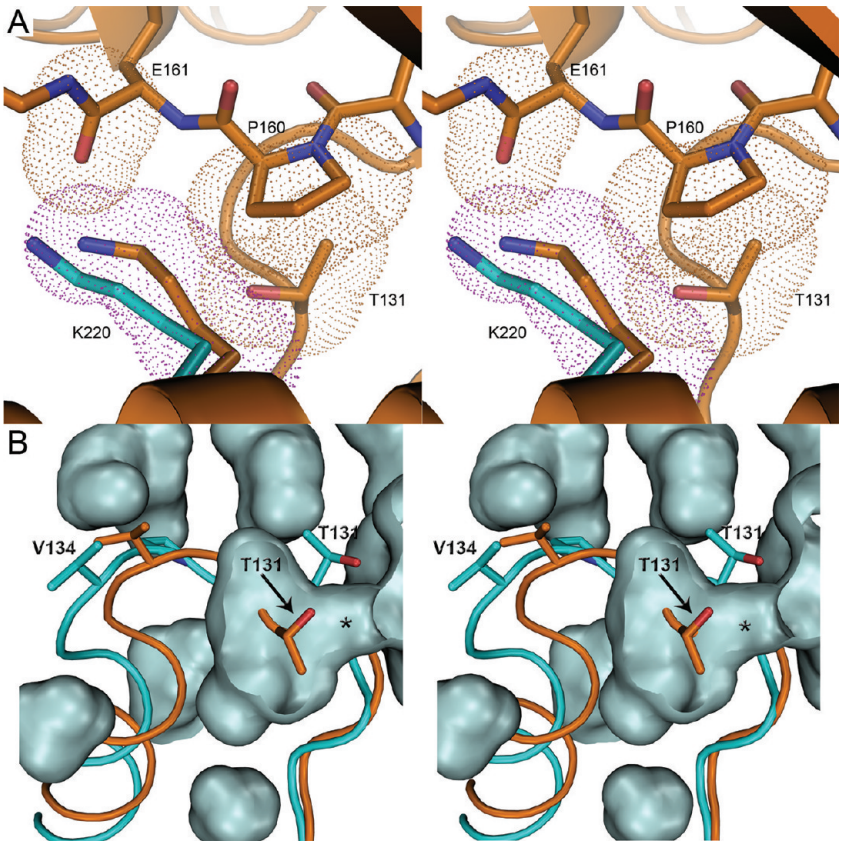

Figure 5. Closed conformation of Δ132 that introduces unfavorable packing interactions. (A) The modeled closed conformation of Δ132 introduces a steric clash between K220 and residues E161, P160, and T131 (orange). The conformation of K220 (teal) in hUGDH:UDG:NADH has shifted to prevent the clash and permit domain closure. (B) Modeling the Δ132 Thr131 loop into the packing environment of the closed conformation (chain L, PDB entry 2Q3E) would bury T131 in a hydrophobic cavity (orange) because of the rotated conformation of the Thr131 loop. The cavity has a volume of ~118 Å^3 and is formed by residues 128−132, 158, 160, 217, and 220. The asterisk identifies a solvent accessible tunnel observed in some chains of hUGDH:UDG:NADH.

Thus, the location of the center of motion can be deduced from a domain flexibility analysis based on the following relationship:[34,35]

$$C_i = \frac{\sum_j ({d_{i,j}}^2 - \overline{d^2})(B_j - \overline{B})}{\left[\sum_j ({d_{i,j}}^2 - \overline{d^2})^2 \sum_j (B_j - \overline{B})^2\right]^{1/2}} \quad (1)$$

where the distance ($d_{i,j}$) from the center of motion (i) is positively correlated (C_i) with the increase in the B factor (B_j) for every atom j. Likewise, atoms that are far from the center of motion will have a strong negative correlation. We considered each C_α atom in the Δ132 crystal structure as a possible center of motion and evaluated eq 1 (Figure 7B). The domain flexibility analysis confirms that the Δ132 construct has three distinct regions of rigid-body mobility, with the NB domain having an overall negative correlation with the rest of the structure (Figure 7B). We repeated this analysis for the hUGDH:UDG:NADH structure (PDB entry 2Q3E) and obtained similar results, albeit without the strong negative correlation of the NB domain seen in Δ132. The negative correlation of the NB domain in the Δ132 structure is due in part to the conformational change; the open conformation of Δ132 increases the average distance of all atoms in the NB domain with respect to the rest of the structure, which according to eq 1 will increase the magnitude of the negative correlation coefficient (provided that the B factors are also increasing).

The largest positive correlation peaks are located in the dimerization domain, consistent with the presence of a hinge axis in that region of the protein (Figure 7B,D). Still, the largest peaks are different between the Δ132 and hUGDH:UDG:NADH structures. Because both the NB and SB domains are flexible, these peaks may represent an "apparent" hinge axis located between two distinct, real axes (Figure 7C, inset). To resolve the possible hinge ambiguity, we divided the Δ132 structure into overlapping N-terminal (residues 1−322) and C-terminal (residues 213−466) fragments, each containing the complete dimerization domain (Figure 7C). Mapping the positive and negative correlation peaks onto the Δ132 structure clearly indicates the motion of the NB and SB domains (Figure 7E). Still, the assignment of an absolute center of motion can be influenced by local dynamics. For example, the hinge-bending axes predicted by DynDom (residues 219−220) are ~16 Å from the center of motion (R298) predicted by the domain flexibility analysis of the N-terminal fragment (Figure 7E). Still, the DynDom-predicted axes are included in center of a cone that radiates from R298 to all of the largest negative correlation peaks in the N-terminal domain (Figure 7E). In the case of hUGDH, the hinge-bending motion appears to be more complex than a single rotation axis. The N- and C-terminal fragments do not identify the same positive correlation peaks, suggesting either (i) two separate centers of motion or (ii) a diffuse center of hinge-bending motion

dx.doi.org/10.1021/bi201381e | *Biochemistry* 2011, 50, 9651−9663

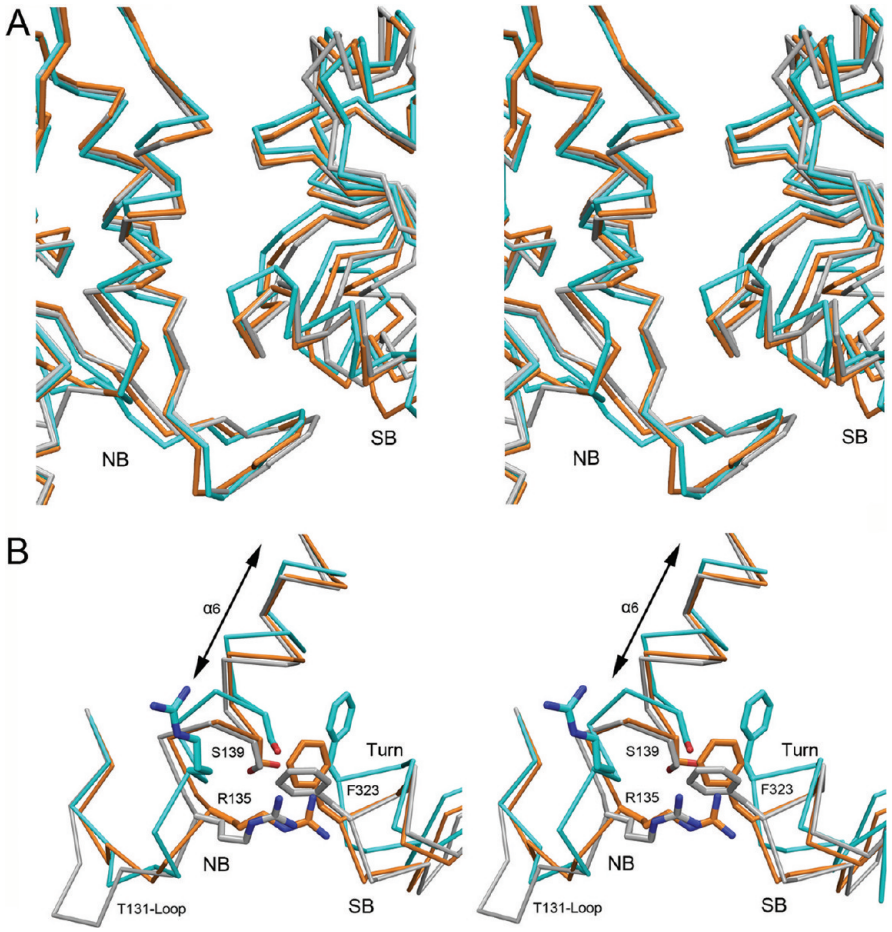

Figure 6. Hexamer-building interface of Δ132 that resembles the UDX-inhibited complex. The C_α atoms of the Δ132 (orange) hexamer-building interface (residues 87−127, 134−155, and 319−460) are superimposed onto the hUGDH:UDG:NADH (teal, PDB entry 2Q3E) and hUGDH−UDX−NAD^+ (gray, PDB entry 3PTZ) structures. (A) Relative orientations of the NB and SB domains from adjacent dimers in the hexamer interface. (B) Key packing interactions in the hexamer-building interface determined by the conformation of the Thr131 loop. The movement of the Thr131 loop rotates the $\alpha 6_{136-144}$ switch helix and changes the packing interactions with the main chain $turn_{322-324}$.

involving a significant portion of the dimerization domain. Modeling the hinge-bending motion of the dimerization domain using the Morphserver supports a diffuse center of motion (Movie S3 of the Supporting Information).

The Δ132 and UDX-Inhibited Structures Have Similar Hexamer-Building Interfaces. The rotation of the NB domain in the Δ132 construct buries ∼200 $Å^2$ more surface in the hexamer-building interface relative to the closed domain conformation of hUGDH:UDG:NADH. The larger interface is consistent with the Δ132 complex forming a more stable hexamer in solution (Figure 2B,C). We have previously reported a correlation between the size of the interface and stability in the UDX-inhibited complex.[13] On the basis of this relationship, we asked if there were additional similarities between the hexamer-building interfaces. To compare the structures, we superimposed 198 corresponding C_α atoms from the domains that make up the hexamer-building interface in the open conformation of Δ132 onto the closed conformations of the following structures: (i) the UDX-inhibited hexamer and (ii) the active hexamer. This analysis shows that the hexamer-building interface of the Δ132 construct is more similar to the inhibited complex than it is to the active hexamer (rmsds of 0.6 and 0.9 Å, respectively). Specifically, the packing interactions between the $\alpha 6_{136-144}$ helix in the NB domain and $turn_{322-324}$ in the SB domain are more similar between the Δ132 and UDX-inhibited hexamer. This is important, because our earlier work identified the $\alpha 6_{136-144}$ helix as the molecular switch that rotates ∼10° to transform the active hexamer to the lower-symmetry, inhibited complex.[13] In contrast, the comparison of Δ132 and hUGDH:UDG:NADH hexamer-building interfaces shows that the $\alpha 6_{136-144}$ switch helix is rotated ∼10° in the latter to favor the high-symmetry conformation (Figure 6B). Likewise, the packing of $turn_{322-324}$ has shifted, and the χ_1 torsion angle of F323 is rotated by ∼22°.

The Conformation of the Thr131 Loop Is Correlated with Domain Rotation. We asked if there was a relationship between domain rotation and the conformation of the Thr131 loop. The hUGDH:UDG:NADH crystal structure contains two hexamers, and all 12 chains adopt the closed conformation. We restricted our analysis of Thr131 loop conformations in the open state to the hUGDH:UGA:NAD^+ (PDB entry 2QG4) and $hUGDH_{E161Q}$ (PDB entry 3KHU) complexes, because these structures do not contain mutations in the Thr131 loop. The hUGDH:UGA:NAD^+ crystal structure contains four dimers. The application of crystallographic symmetry shows that each unique dimer forms a hexameric complex displaying an "open−closed" asymmetry with respect to the conformation of the NB domain; the top "trimer" of each hexamer (chains A, C, E, and G) adopts an open conformation with a bending angle of 11.4°, while the bottom three molecules (chains B, D, F, and H) are in the closed state (Figure 8A). This asymmetry may be related to earlier

dx.doi.org/10.1021/bi201381e | *Biochemistry* 2011, 50, 9651−9663

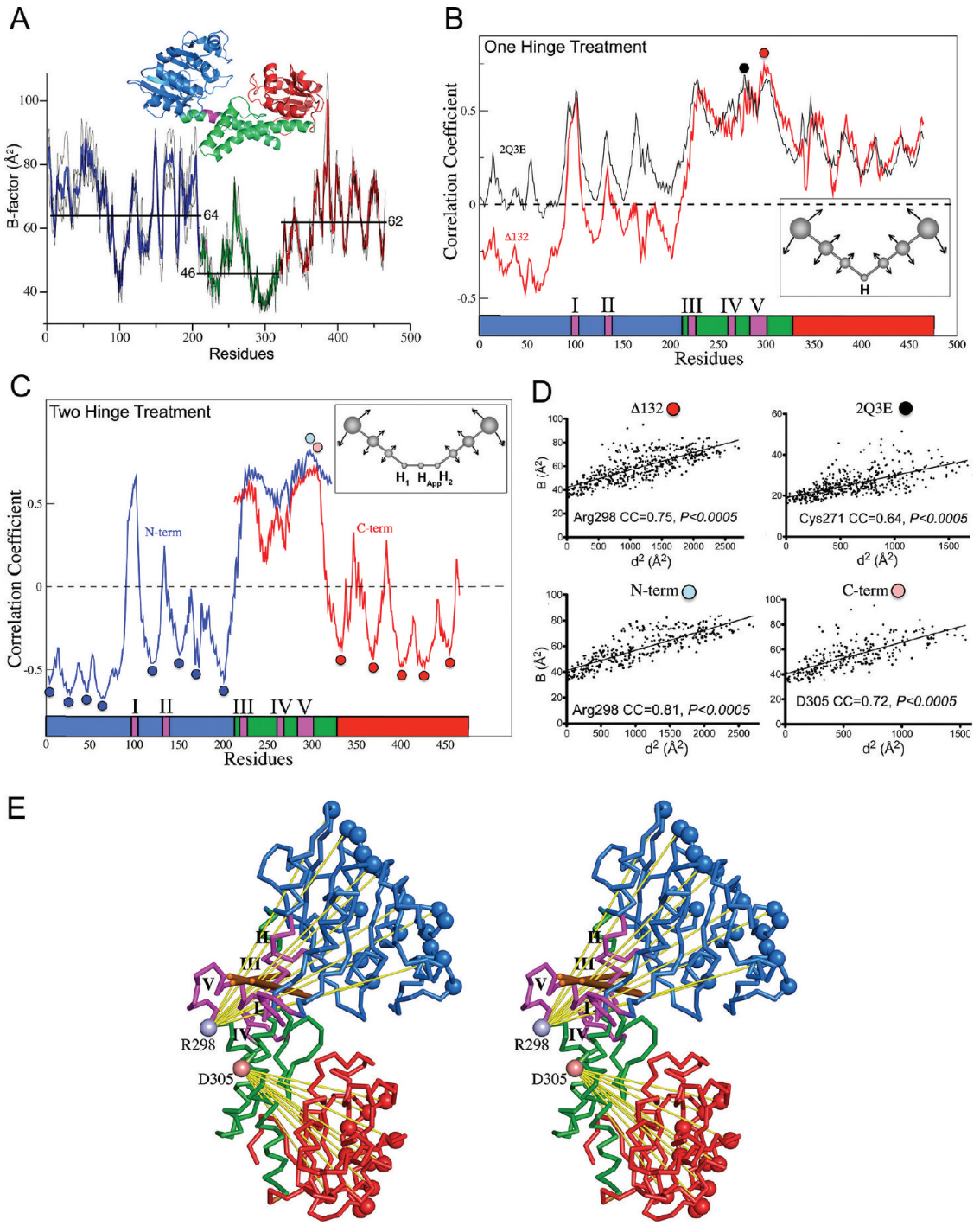

Figure 7. Domain flexibility in hexameric hUGDH. For this analysis, the final structures were re-refined without TLS parameters. (A) Average *B* factors of the Δ132 C_α atoms plotted as a line colored by domain: NB (blue), dimerization (green), and SB (red). The hinge axis predicted by DynDom is shown as a purple line. The *B* factors for each chain in the asymmetric unit are also plotted as thin black lines. (B) Plot showing the correlation of *B* factors with linear distance (eq 1) from each residue in Δ132 (red) and hUGDH:UDG:NADH (black). Colored bars indicate the domain structure as described in Figure 1, with the potential hinge-bending regions I-V colored purple. The inset shows the one-hinge model for the correlation of increasing *B* factors (arrows of increasing length) with the linear distance from a hinge axis, *H*. The residues predicted to be near the center of motion are depicted as red and black circles for Δ132 and hUGDH:UDG:NADH, respectively. (C) Treating Δ132 to a two-hinge analysis by analyzing overlapping N-terminal (residues 1−322, blue) and C-terminal (residues 213−466, red) fragments. The inset presents the two-hinge model; the separation of the two mobile domains can result in an apparent hinge axis (H_{App}) between the two real axes (H_1 and H_2). The residues predicted to be near the center of motion are depicted as light blue and light red circles for the N- and C-terminal fragments, respectively. Residues with large, negative correlations are shown as dark blue circles (N-terminus) and dark red circles (C-terminus). (D) Centers of motion predicted in panels C and D fit to eq 1. (E) Comparison of the hinge axes and the hinge regions from Figure 4C to the centers of motion predicted in panel D (light blue and red spheres for the N- and C-terminal fragments, respectively). The residues farthest from the center of motion (dark spheres) are shown. The linear distances between the centers of motion and some of the negatively correlated residues (dark spheres) are depicted as yellow lines.

dx.doi.org/10.1021/bi201381e | *Biochemistry* 2011, 50, 9651−9663

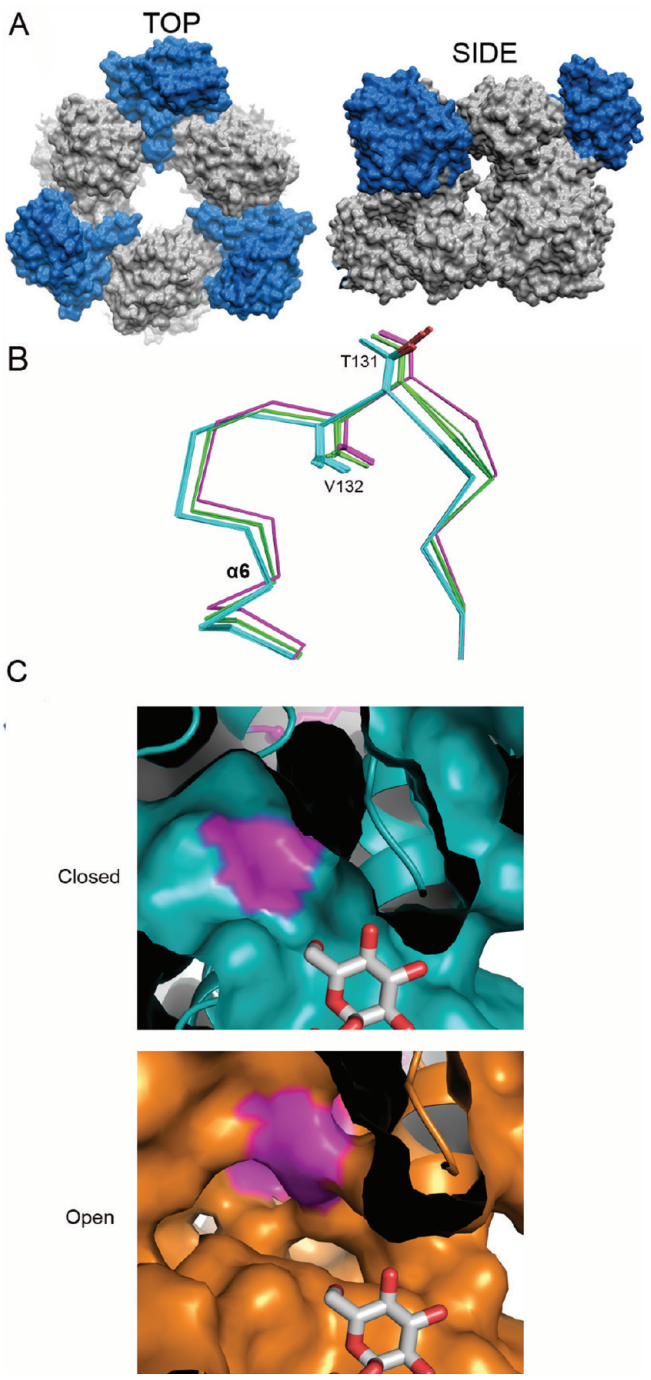

Figure 8. Domain rotation is correlated with the conformation of the Thr131 loop. (A) Top and side views of the hUGDH:UGA:NAD^+ solvent accessible surface (PDB entry 2QG4) showing the asymmetry of the domain conformation. The open NB domains are colored blue. (B) Superposition of the Thr131 loops from hUGDH:UDG:NADH, hUGDH:UGA:NAD^+, and $hUGDH_{E161Q}$ (PDB entries 2Q3E, 2QG4, and 3KHU, respectively). The Thr131 loops are colored according to NB domain conformation: (i) teal, closed for hUGDH:UDG:NADH (chains A–L) and hUGDH:UGA:NAD^+ (chains B, D, F, and H); green, open for hUGDH:UGA:NAD^+ (chains A, C, E, and G); and purple, open $hUGDH_{E161Q}$ (chains A–F). The $\alpha 6$ switch helix is identified. (C) Rotation of the NB and SB domains increases the solvent exposure of the Thr131 loop (purple). The closed conformation of hUGDH:UDG:NADH and the modeled open conformation show the increase in solvent exposure of the binding pocket due to domain opening.

reports of half-of-the-sites activity,[36−38] but additional evidence is needed to support this model. In contrast, all six chains of the $hUGDH_{E161Q}$ hexamer show a hinge opening of 9° (Table 2).

To compare the different structures, we superimposed the main chain atoms of residues 1−124 to remove bias from any real conformational differences in the Thr131 loop and $\alpha 6_{136-144}$ helix. Superpositions of the 8 hUGDH:UGA:NAD^+, 12 hUGDH:UDG:NADH, and 6 $hUGDH_{E161Q}$ monomers using residues 1−124 yielded rmsds of no more than 0.47 Å, which is within the expected range of the coordinate error for these structures. All of the monomers with closed domains (12 from hUGDH:UDG:NADH and 4 from hUGDH:UGA:NAD^+) reveal the same conformation of the Thr131 loop (Figure 8B). In contrast, the Thr131 loops in the open domains adopt two distinct conformations observed in (Figure 8B) (i) the four monomers of the hUGDH:UGA:NAD^+ structure and (ii) the six chains of the $hUGDH_{E161Q}$ structure. The $hUGDH_{E161Q}$ complex is unique in that it contains a covalent reaction intermediate bound to the active site nucleophile, C276. Unlike the Δ132 structure, all of the $\alpha 6_{136-144}$ switch helices adopt the conformation that favors the high-symmetry, active hexamer.

To measure changes in the solvent accessibility of the Thr131 loop due to domain rotation, we modeled wild-type hUGDH:UDG:NADH in the open conformation. Using the Δ132 structure as a template, we superimposed the NB domain fragment (residues 1−212) and the C-terminal fragment (residues 213−466) of hUGDH:UDG:NADH (similar to our modeling of the closed conformation of the Δ132 structure in the preceding section). This modeling experiment shows that the rotation of the NB domain increases the solvent accessible surface of the Thr131 loop by 62% (Figure 8C and Table 3).

Table 3. Contact Area of the Thr131 Loop

	Thr131 loop contact area ($Å^2$)[a]		
residue	closed	open	fully exposed
128	0.5	0.6	57.45
129	2.2	2.2	61.21
130	3.5	3.5	26.15
131	5.2	14.7	43.67
132	1.2	1.7	21.18
133	7.2	8.7	34.96
134	3.0	10.3	44.07
135	22.6	31.3	83.39
total	45.4	73.0	372.08

[a]The contact area was calculated using a 1.4 Å probe.

DISCUSSION

Hinge Bending Facilitates the Repacking of the Thr131 Loop in the Protein Core. The allokleidic response of hUGDH involves a repacking of the protein core that disrupts the symmetry of the hexameric complex (Figure 1).[13] Our previous work showed that the evolution of hUGDH selected for large buried cavities to accommodate the two distinct conformations of the Thr131 loop in the protein core.[13] The goal of this study was to determine how the Thr131 loop overcomes the steric constraints of the core to switch

dx.doi.org/10.1021/bi201381e | Biochemistry 2011, 50, 9651−9663

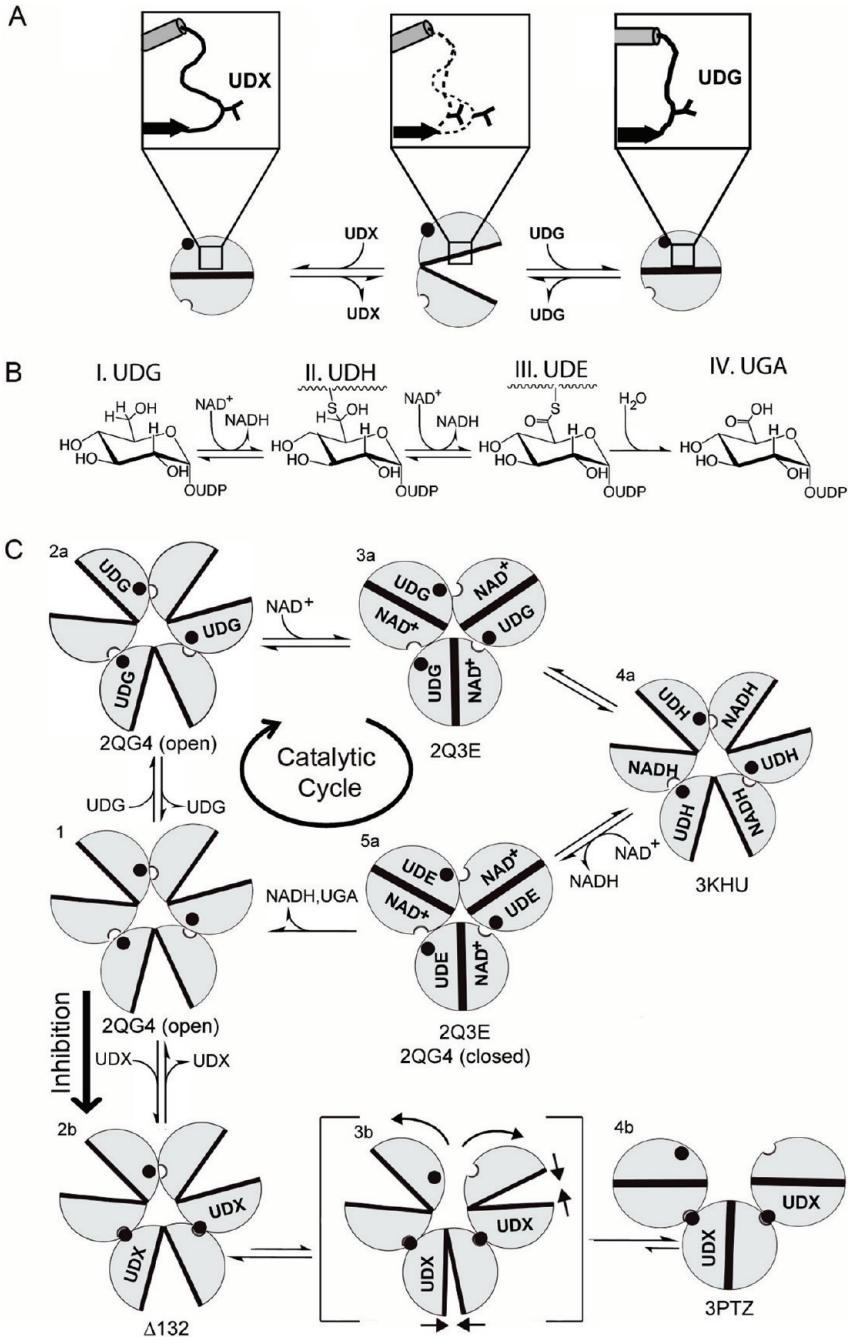

Figure 9. Model for the allokleidic regulation of hUGDH. (A) hUGDH is depicted as a circle that undergoes a clamshell-like opening. The top and bottom halves of the circle represent the NB and SB domains, respectively. The dark circle in the NB domain represents the α6 switch helix, and the semicircular cutout in the SB domain is $turn_{322-324}$ (see Figure 6B). Close-up insets illustrate the Thr131 loop and α6 switch helix in ordered (—) and flexible (---) conformations. Domain opening allows the Thr131 loop to repack in response to UDX or UDG. (B) Reaction mechanism of hUGDH. In steps I and II, NAD^+ oxidizes C6′ of UDG, which is then attacked by C276 to form a thiohemiacetal intermediate (UDH). In steps II and III, NAD^+ oxidizes C6′ of UDH to a thioester (UDE). In steps III and IV, hydrolysis of the thioester releases the products UGA and NADH. (C) Catalytic cycle and UDX inhibition of hUGDH. hUGDH is represented by a trimer of the clamshell circles described in panel A. For the sake of simplicity, only the top trimer of the hUGDH hexamer is depicted. Substrates, intermediates, and products illustrated in panel B are shown bound in the appropriate domains. In the catalytic cycle, domain rotation (open clamshells) facilitates substrate−product exchange. In feedback inhibition, UDX binds in two of the subunits and shifts the associated α6 switch helix (black circles) to strengthen the packing interactions (semicircular cutout) in the adjacent SB domains (step 2b). The bracketed structure (step 3b) illustrates the dissociation of the remaining weak interface (curved arrows) and the closing (straight arrows) of the two UDX-bound subunits to maximize the interactions of the protein with the inhibitor. The PDB entries that support each proposed conformation of this model are listed under the appropriate intermediates.

between the alternate packing conformations (Figure 1C,D). To address this, we took the unusual step of deleting a buried core residue from the Thr131 loop to approximate an intermediate conformation in the transition. Deleting a buried residue is tantamount to performing a mass substitution of core residues. Despite this, the high-level expression and solubility of the Δ132 construct are good indicators that the deletion is tolerated by the structure.

The deletion of V132 caused the NB domain to rotate to an open conformation. By comparing the open and closed forms of hUGDH, we identified a single hinge-bending axis between residues 218 and 224 in the dimerization domain (Figure 4). This agrees with a previous study that first documented the hinge-bending motion for the NB domain in hUGDH.[14] We used Morphserver[32] to model the transition between the open and closed conformations (Movies S1−S3 of the Supporting Information). This modeling experiment suggested that there might be a separate motion associated with the movement of the SB domain. Comparing structures to identify a hinge-bending motion is limited to the conformations selected by the crystal lattice. We extended our analysis of the motion using an orthogonal approach based on a single structure: the correlation of *B* factors with the linear distance from a hinge axis to identify centers of domain flexibility.[34,35] Using this technique, we identified a separate center of motion for each of the terminal domains. The center of motion predicted for the NB domain included the hinge-bending axes identified by comparing crystal structures (Figure 7E). Moreover, the domain flexibility analysis agrees with our modeling studies by identifying a separate center of motion for the SB domain (Movie S3 of the Supporting Information). We propose that rotation of the NB and SB domains to the open conformation involves at least two centers of motion located in the dimerization domain. The open conformation removes the steric packing constraints that would prevent the allokleidic response (Figure 8C and Table 3). In fact, our analysis shows that the conformation of the Thr131 loop is correlated with the rotation of the NB domain in wild-type hUGDH (Figure 8B). Thus, we propose that domain rotation is the essential step in the repacking of the Thr131 loop and the protein core in response to the feedback inhibitor UDX (Figure 9A).

Domain Rotation Can Occur without Disrupting the Hexamer. The catalytic mechanism for UGDH requires two molecules of NAD^+ to oxidize UDG to UGA[1,39] (Figure 9B). Recently, it has been suggested that rotation of the NB domain facilitates the NADH−NAD^+ exchange during the catalytic cycle[14,40] (Figure 9C). The previous studies did not address whether domain rotation could occur in the context of the hexamer. Because all of the hUGDH crystal structures are hexamers, we were able to analyze the pattern of main chain flexibility of the NB and SB domains while packed in the hexamer-building interface. This analysis shows that the NB and SB domains behave as flexible rigid bodies (Figure 7A). Because the NB and SB domains are in contact in the hexamer interface, the close correlation of the average *B* factors (64 and 62 $Å^2$, respectively) is strong evidence that the domains move in a concerted fashion. Modeling the domain motion in the hexamer supports our argument that the opening motion of the domains is correlated (Movies S1 and S2 of the Supporting Information). We believe that the NB and SB domains rotate in a concerted motion to form the distinct hexamer-building interfaces of the open and closed conformations without disrupting the oligomeric complex. This is important for substrate−product exchange, assuming the hexameric state is required for catalysis (Figure 9C).

Role of Domain Rotation in the Transition between Hexameric States. Domain rotation is essential to the allokleidic mechanism of hUGDH. We have shown that (i) domain rotation removes the steric constraints that would otherwise prevent the movement of the Thr131 loop (Figures 8C and 9A), (ii) both the NB and SB domains can move in a concerted fashion without disrupting the hexamer (Figures 6 and 7 and Movies S1 and S2 of the Supporting Information), and (iii) the open conformation of hUGDH has a hexamer-building interface similar to that of the UDX-inhibited, low-symmetry complex (Figure 6). But how does the remarkable transition from the high- to low-symmetry hexamer occur? On the basis of our results, we propose a structurally detailed model for the allokleidic transition of hUGDH (Figure 9C). The first step to forming the inhibited hexamer involves the concerted rotation of the NB and SB domains to the open conformation (Figure 9C, step 1). Evidence of this comes from the open conformation of the hUGDH:UGA:NAD^+ structure. This structure has an interface similar to that of the inhibited hexamer, but without the critical rotation of the $\alpha6_{136-144}$ switch helix (Figure 8B). In the next step, UDX binds to the open conformation and elicits an induced-fit response that rotates the $\alpha6_{136-144}$ switch helix (Figure 9C, step 2b). Support for this step comes from the Δ132 structure, in which the deletion of V132 has shortened the Thr131 loop to mimic the induced-fit response to UDX binding (Figure 3C). As a result, the $\alpha6_{136-144}$ switch helix has rotated to the conformation that favors the inhibited structure (Figures 3C and 6). It is fortuitous that the deletion of V132 trapped the structure in the open domain conformation, which is essential for the loop to move in this this critical step of the allokleidic transition. But how does UDX binding disrupt the symmetry of the hexamer in the final step (Figure 9C, step 3b)? Like the deletion of V132, UDX binding also rotates the $\alpha6_{136-144}$ helix to strengthen the adjacent hexamer-building interface (Figure 2B,C).[13] Our previous crystal structure of the inhibited hUGDH had UDX bound in all of the active sites, most likely because of the high concentrations (5 mM) of UDX during crystallization. We believe that a hexamer not fully saturated with UDX would preferentially dissociate along the weakest interface (Figure 9C, step 2b). The domains containing UDX would favor the closed conformation to maximize the interactions of the protein with the inhibitor.[13] Thus, in adopting the closed domain conformation, the entire dimer would appear to rotate and form the inhibited complex (Figure 9C, step 3c). This model shows that domain rotation is an integral part of the induced-fit response to UDX and the formation of the inhibited hexamer. We believe that domain rotation originated as a means for substrate exchange, and that this attribute was subsequently adapted to facilitate the allokleidic response.

■ ASSOCIATED CONTENT

Ⓢ Supporting Information

Additional information about domain motion in hUGDH homologues as well as MorphServer movies illustrating domain motion in hUGDH. This material is available free of charge via the Internet at http://pubs.acs.org.

Accession Codes

The atomic coordinates and structure factors have been deposited in the Protein Data Bank as entry 3TF5.

■ AUTHOR INFORMATION

Corresponding Author

*Phone: (706) 583-0304. Fax: (706) 542-1738. E-mail: zac@bmb.uga.edu.

Funding

Funding from American Cancer Society Grant RSG0918401DMC and the University of Georgia Research Alliance to Z.A.W. is gratefully acknowledged.

■ ACKNOWLEDGMENTS

We thank the SER-CAT beamline personnel (Advanced Photon Source, Argonne National Laboratory) for help with data collection. We also thank Mr. William B. Peeples for helpful comments during the writing of the manuscript.

■ ABBREVIATIONS

hUGDH, human UDP-α-D-glucose 6-dehydrogenase; UDG, UDP-α-D-glucose; UGA, UDP-α-D-glucuronic acid; UDH, UDP-α-D-6-thioglucose; UDE, UDP-α-D-6-thioglucohexodialdo-1,5-pyranose; UDX, UDP-α-D-xylose; NB, NAD^+ binding domain; SB, UDP sugar binding domain; PDB, Protein Data Bank.

■ REFERENCES

(1) Kalckar, H., Maxwell, E., and Strominger, J. (1956) Some properties of uridine diphosphoglucose dehydrogenase. *Arch. Biochem. Biophys. 65*, 2−10.

(2) Esko, J. D., Kimata, K., and Lindahl, U. (2009) Proteoglycans and Sulfated Glycosaminoglycans. In *Essentials of Glycobiology* (Varki, A., Cummings, R. D., Esko, J. D., Freeze, H. H., Stanley, P., Bertozzi, C. R., Hart, G. W., and Etzler, M. E., Eds.) 2nd ed., Cold Spring Harbor Labratory Press, Plainview, NY.

(3) Zhang, L. (2010) Glycosaminoglycan (GAG) biosynthesis and GAG-binding proteins. *Prog. Mol. Biol. Transl. Sci. 93*, 1−17.

(4) Sironen, R. K., Tammi, M., Tammi, R., Auvinen, P. K., Anttila, M., and Kosma, V. M. (2011) Hyaluronan in human malignancies. *Exp. Cell Res. 317*, 383−391.

(5) Yamada, S., and Sugahara, K. (2008) Potential therapeutic application of chondroitin sulfate/dermatan sulfate. *Curr. Drug Discovery Technol. 5*, 289−301.

(6) Theocharis, A. D., Skandalis, S. S., Tzanakakis, G. N., and Karamanos, N. K. (2010) Proteoglycans in health and disease: Novel roles for proteoglycans in malignancy and their pharmacological targeting. *FEBS J. 277*, 3904−3923.

(7) Corte, M. D., Gonzalez, L. O., Junquera, S., Bongera, M., Allende, M. T., and Vizoso, F. J. (2010) Analysis of the expression of hyaluronan in intraductal and invasive carcinomas of the breast. *J. Cancer Res. Clin. Oncol. 136*, 745−750.

(8) Udabage, L., Brownlee, G. R., Waltham, M., Blick, T., Walker, E. C., Heldin, P., Nilsson, S. K., Thompson, E. W., and Brown, T. J. (2005) Antisense-mediated suppression of hyaluronan synthase 2 inhibits the tumorigenesis and progression of breast cancer. *Cancer Res. 65*, 6139−6150.

(9) Liu, N., Gao, F., Han, Z., Xu, X., Underhill, C. B., and Zhang, L. (2001) Hyaluronan synthase 3 overexpression promotes the growth of TSU prostate cancer cells. *Cancer Res. 61*, 5207−5214.

(10) Lai, E., Singh, R., Teng, B., Zhao, Y., Sharratt, E., Howell, G., Rajput, A., and Bullard Dunn, K. (2010) Inhibition of hyaluronan synthase-3 decreases subcutaneous colon cancer growth in mice. *Dis. Colon Rectum 53*, 475−482.

(11) Itano, N., Sawai, T., Miyaishi, O., and Kimata, K. (1999) Relationship between hyaluronan production and metastatic potential of mouse mammary carcinoma cells. *Cancer Res. 59*, 2499−2504.

(12) Wang, T.-P., Pan, Y.-R., Fu, C.-Y., and Chang, H.-Y. (2010) Down-regulation of UDP-glucose dehydrogenase affects glycosaminoglycans synthesis and motility in HCT-8 colorectal carcinoma cells. *Exp. Cell Res. 316*, 2893−2902.

(13) Kadirvelraj, R., Sennett, N. C., Polizzi, S. J., Weitzel, S., and Wood, Z. A. (2011) Role of packing defects in the evolution of allostery and induced fit in human UDP-glucose dehydrogenase. *Biochemistry 50*, 5780−5789.

(14) Egger, S., Chaikuad, A., Kavanagh, K. L., Oppermann, U., and Nidetzky, B. (2011) Structure and mechanism of human UDP-glucose 6-dehydrogenase. *J. Biol. Chem. 286*, 23877−23887.

(15) Neufeld, E. F., and Hall, C. W. (1965) Inhibition of UDP-D-glucose Dehydrogenase by UDP-D-xylose: A Possible Regulatory Mechansim. *Biochem. Biophys. Res. Commun. 19*, 456−461.

(16) Kabsch, W. (2010) Xds. *Acta Crystallogr. D66*, 125−132.

(17) Vagin, A., and Teplyakov, A. (2010) Molecular replacement with MOLREP. *Acta Crystallogr. D66*, 22−25.

(18) Vagin, A. A., Steiner, R. A., Lebedev, A. A., Potterton, L., McNicholas, S., Long, F., and Murshudov, G. N. (2004) REFMAC5 dictionary: Organization of prior chemical knowledge and guidelines for its use. *Acta Crystallogr. D60*, 2184−2195.

(19) Emsley, P., and Cowtan, K. (2004) Coot: Model-building tools for molecular graphics. *Acta Crystallogr. D60*, 2126−2132.

(20) Vagin, A. A., Steiner, R. A., Lebedev, A. A., Potterton, L., McNicholas, S., Long, F., and Murshudov, G. N. (2004) REFMAC5 dictionary: Organization of prior chemical knowledge and guidelines for its use. *Acta Crystallogr. D60*, 2184−2195.

(21) Brunger, A. T., and Rice, L. M. (1997) Crystallographic refinement by simulated annealing: Methods and applications. *Methods Enzymol. 277*, 243−269.

(22) Laue, T. M., Shah, B. D., Ridgeway, T. M., and Pelletier, S. L. (1992) Computer-aided interpretation of analytical sedimentation data for proteins. In *Analytical ultracentrifugation in biochemistry and polymer science* (Harding, S. E., Rowe, A. J., and Horton, J. C., Eds.) The Royal Society of Chemistry, Cambridge, U.K.

(23) Schuck, P. (2003) On the analysis of protein self-association by sedimentation velocity analytical ultracentrifugation. *Anal. Biochem. 320*, 104−124.

(24) Wilson, D. (1965) Purification of uridine diphosphoglucose dehydrogenase from calf liver. *Anal. Biochem. 10*, 472−478.

(25) Campbell, R. E., Mosimann, S. C., van De Rijn, I., Tanner, M. E., and Strynadka, N. C. (2000) The first structure of UDP-glucose dehydrogenase reveals the catalytic residues necessary for the two-fold oxidation. *Biochemistry 39*, 7012−7023.

(26) Richards, F. M., and Kundrot, C. E. (1988) Identification of structural motifs from protein coordinate data: Secondary structure and first-level supersecondary structure. *Proteins 3*, 71−84.

(27) DeDecker, B. S., O'Brien, R., Fleming, P. J., Geiger, J. H., Jackson, S. P., and Sigler, P. B. (1996) The crystal structure of a hyperthermophilic archaeal TATA-box binding protein. *J. Mol. Biol. 264*, 1072−1084.

(28) Hayward, S., and Berendsen, H. J. (1998) Systematic analysis of domain motions in proteins from conformational change: New results on citrate synthase and T4 lysozyme. *Proteins 30*, 144−154.

(29) Holm, L., and Rosenstrom, P. (2010) Dali server: Conservation mapping in 3D. *Nucleic Acids Res. 38*, W545−W549.

(30) Blaber, M., Lindstrom, J. D., Gassner, N., Xu, J., Heinz, D. W., and Matthews, B. W. (1993) Energetic cost and structural consequences of burying a hydroxyl group within the core of a protein determined from Ala → Ser and Val → Thr substitutions in T4 lysozyme. *Biochemistry 32*, 11363−11373.

(31) Kumar, M. D., and Gromiha, M. M. (2006) PINT: Protein-protein Interactions Thermodynamic Database. *Nucleic Acids Res. 34*, D195−D198.

(32) Krebs, W. G., and Gerstein, M. (2000) The morph server: A standardized system for analyzing and visualizing macromolecular motions in a database framework. *Nucleic Acids Res. 28*, 1665−1675.

(33) Trueblood, K. N., Burgi, H.-B., Burzlaff, H., Dunitz, J. D., Gramaccioli, C. M., Schulz, H. H., Shmueli, U., and Abrahams, S. C. (1996) Atomic Dispacement Parameter Nomenclature. Report of a Subcommittee on Atomic Displacement Parameter Nomenclature. *Acta Crystallogr. A52*, 770−781.

(34) Sternberg, M. J., Grace, D. E., and Phillips, D. C. (1979) Dynamic information from protein crystallography. An analysis of temperature factors from refinement of the hen egg-white lysozyme structure. *J. Mol. Biol. 130*, 231−252.

(35) Weaver, L. H., and Matthews, B. W. (1987) Structure of bacteriophage T4 lysozyme refined at 1.7 Å resolution. *J. Mol. Biol. 193*, 189−199.

(36) Franzen, J. S., Marchetti, P., Ishman, R., and Ashcom, J. (1978) Half-sites oxidation of bovine liver uridine diphosphate glucose dehydrogenase. *Biochem. J. 173*, 701−704.
(37) Eccleston, E. D., Thayer, M. L., and Kirkwood, S. (1979) Mechanisms of action of histidinol dehydrogenase and UDP-Glc dehydrogenase. Evidence that the half-reactions proceed on separate subunits. *J. Biol. Chem. 254*, 11399−11404.
(38) Franzen, J. S., Ashcom, J., Marchetti, P., Cardamone, J. J. Jr., and Feingold, D. S. (1980) Induced versus pre-existing asymmetry models for the half-of-the-sites reactivity effect in bovine liver uridine diphosphoglucose dehydrogenase. *Biochim. Biophys. Acta 614*, 242−255.
(39) Ge, X., Penney, L. C., van de Rijn, I., and Tanner, M. E. (2004) Active site residues and mechanism of UDP-glucose dehydrogenase. *Eur. J. Biochem. 271*, 14−22.
(40) Campbell, R. E., Mosimann, S. C., van de Rijn, I., Tanner, M. E., and Strynadka, N. C. (2000) The first structure of UDP-glucose dehydrogenase reveals the catalytic residues necessary for the two-fold oxidation. *Biochemistry 39*, 7012−7023.
(41) Diederichs, K., and Karplus, P. A. (1997) Improved R-factors for diffraction data analysis in macromolecular crystallography. *Nat. Struct. Biol. 4*, 269−275.
(42) Weiss, M. S., and Hilgenfeld, R. (1997) On the use of the merging R factor as a quality indicator for X-ray data. *J. Appl. Crystallogr. 30*, 203−205.
(43) Ge, X., Penney, L., van de Rijn, I., and Tanner, M. (2004) Active site residues and mechanism of UDP-glucose dehydrogenase. *Eur. J. Biochem. 271*, 14−22.